



Trade Science Inc.

ISSN : 0974 - 7478

Volume 7 Issue 3

Macromolecules

An Indian Journal

Microreview

MMAIJ, 7(3), 2011 [126-138]

Recent developments in clay-containing polymeric nanocomposites: Clay characterization & high pressure dilatometry

L.A.Utracki

National Research Council Canada, Industrial Materials Institute, 75 de Mortagne, Boucherville, QC, J4B 6Y4, (CANADA)

E-mail: leszek.utracki@cnrc-nrc.gc.ca

Received: 24th August, 2011 ; Accepted: 24th September, 2011

ABSTRACT

In structural clay-containing polymeric nanocomposites (CPNC) ca. 2 – 5 wt% clay is dispersed in polymer matrix: thermoplastic, thermoset or elastomeric. Since most clay/polymer systems are antagonistically immiscible, in analogy to immiscible polymer blends a two-step compatibilization is required: (1) intercalation transforming clay into organoclay and (2) addition of functional compatibilizer(s). The volume of these compatibilizing species usually is larger than that of clay itself. These additives affect the thermodynamic, rheology and other performance characteristics of CPNC. Since the system is immiscible, i.e., sensitive to stresses during compounding and forming, the reproducibility of behavior may be a problem. Furthermore, from the chemical and physical points of view the natural and synthetic clays are complex. The purified natural clay may contain 2-5 wt% contaminants (humic derivatives, quartz, gypsum, dolomite, and other minerals), whereas the synthetic ones may be mixtures of different crystallographic forms (e.g., lamellar and needle-like). Crystalline clays, natural or not, have polydispersed platelets shapes and sizes. Accordingly, characterization of CPNC should start with that of a clay, its platelet size, their inherent dispersibility (absence of interlamellar crystalline welding) and presence of contaminants. CPNC are being characterized by the rheological methods in the solid and molten state. Their mechanical, barrier, dielectric and other properties are determined following the standard methods. However, the use of the high pressure dilatometry (HPD) is rare, even when this is the simplest way for determining the free volume and the thermodynamic interaction parameters as well as the key thermodynamic and engineering quantities, e.g., the thermal expansion and compressibility coefficients. The HPD measurements are important, especially in view of the kinetic nature of the transitions (vitrification, crystallization) that stretches into the non-equilibrium melt. An overview of the method and results obtained for CPNC with amorphous or semi-crystalline polymeric matrices are described. © 2011 Trade Science Inc. - INDIA

CHARACTERIZATION OF CLAY

The clay-containing polymeric nanocomposites (CPNC) are dispersions of clay in a polymer. For good performance the exfoliation is desired. In industrial manufacture of the structural CPNC the crystalline clays, natural or synthetic, are used. The clay platelets are 0.7 – 1.7 nm thick with the aspect ratio: $p = \text{diameter/thickness} = 20 - 6000^{[1]}$. The natural clays are

contaminated with (1) organic (e.g., humic substances, HS), (2) parasitic clays (e.g., amorphous or non-expandable) and (3) particulate minerals (quartz, sand, silt, feldspar, gypsum, orthoclase, apatite, calcite, dolomite, biotite, etc.).

CPNC manufacture involves melt compounding in a single or twin-screw extruder (SSE or TSE, respectively) in the shear or extensional flow field. Dispersing in extensional flow is more energy-efficient,

generates better dispersive and distributive mixing, is performed in a more uniform stress field at lower temperatures and it does not re-aggregate solid particles as the shear field does. Some years back an extensional flow mixer (EFM) and its dynamic version, DEFM were developed. These devices may be attached to a SSE or TSE, or used as the stand-alone mixers^[2]. The key requirement for a CPNC clay is its ability for exfoliating, related to the ionic imbalance of the crystalline layers, which must be compensated by hydrated ions in the interlayer galleries. The most important (natural or synthetic) exfoliating clays are: montmorillonite (MMT), hectorite (HT), and saponite (SP). These minerals have an octahedral layer (Oc) sandwiched between two tetrahedral (Tc) ones. These sandwiches are separated by aqueous counter-ion layers. The synthetic clays are classified as^[3]:

- Semi-synthetic, prepared by reacting natural mineral with salts.
- Synthetic, formed in a high temperature reaction between metal salts or oxides.
- Templated, starting with organic templates, which after synthesis may be pyrolyzed.

In the recent VAMAS TWA-33 project three types of sodium-clays were studied^[4]: (1) the natural MMT, Cloisite[®]-Na⁺ (C-Na⁺), (2) the semi-synthetic fluorohectorite, Somasif ME-100, and (3) the synthetic fluorotetrasilicic mica, Topy-Na⁺. Their properties are listed in TABLE 1.

TABLE 1 : Properties of the sodium-clays.

Property	C-Na ⁺	ME-100	Topy-Na ⁺
Specific density, g/mL	2.86	2.6	2.6
Interlayer spacing, d_{001} (nm)	1.17	0.95	1.23
Platelets thickness, nm	0.96	0.91	
CEC (meq/g)	0.92	1.2	0.80
Nominal aspect ratio, p (-)	280	≤ 6000	≤ 5000

The clays were characterized for the platelet shape, size, chemical composition and presence of impurities. The test procedures and results were published^[4]. Examples of ME-100 images are shown in Figure 1. The number and weight average values of the platelet length and the orthogonal width (subscripts n and w , respectively) are listed in TABLE 2. The average clay platelet dimensions in three orthogonal directions are: thickness $t \approx 1$ nm, width $W \approx 20 - 4000$ nm, length $L \approx 30 - 6000$ nm, with the nearly universal ratio $L/W \approx 1.5 \pm 0.1$. The distribution of clay platelet size is nearly Gaussian.

Chemical analysis of clays was obtained by the energy-dispersive X-ray (EDX) analysis in SEM. Since

TABLE 2 : Statistical analysis of three clays.

Clay	Length L (nm)		Width, W (nm)		Ratios	
	L_n	L_w	W_n	W_w	$(L/W)_n$	$(L/W)_w$
Natural, C-Na ⁺	290	350	183	219	1.58	1.60
Semi-synthetic, ME-100	872	1097	572	743	1.52	1.48
Synthetic, Topy-Na ⁺	1204	1704	761	1186	1.58	1.44
Error					± 0.2	± 0.2

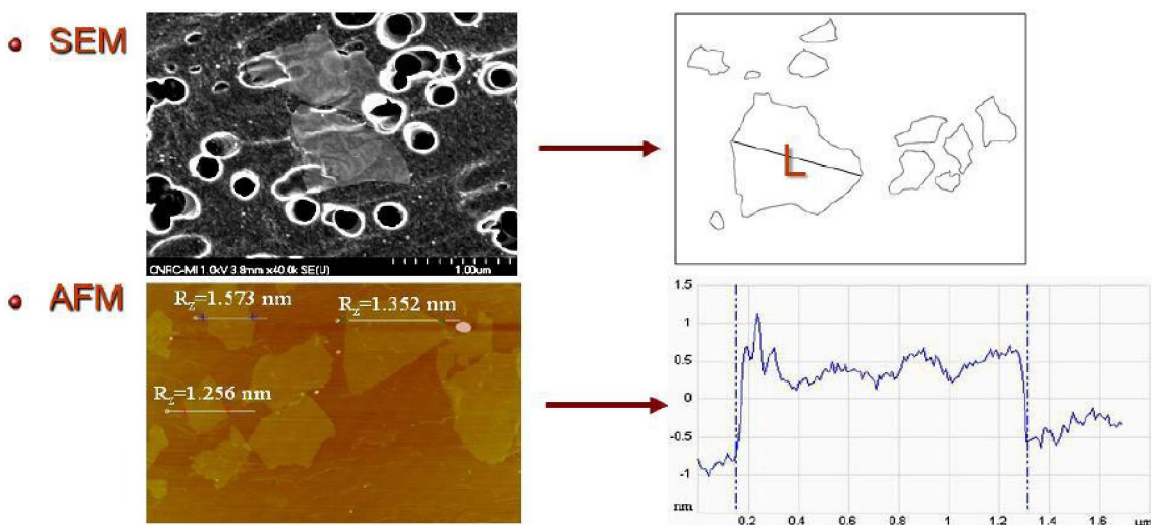


Figure 1 : Scanning electron microscopy (SEM) and atomic force microscopy (AFM) images of Somasif ME-100 platelets. As an example, the platelet length is indicated as L ; the width, W , is taken as the largest perpendicular to L ^[4].

Microreview

clay particles may have locally different composition, ca. 30 particles were sampled at least at five locations, each. Results are listed in TABLE 3.

TABLE 3 : Elemental composition of C-Na⁺ and ME-100 clays^[4].

Source	C-Na ⁺	ME-100
Nominal	[Al _{3.34} Mg _{0.66} Na _{0.66}] (Si ₈ O ₂₀)(OH) ₄	(NaF) _{2.2} (MgF ₂) _{0.1} (MgO) _{5.4} (SiO ₂) ₈
Found	[Al _{2.9} Fe _{0.6} Mg _{0.35} Na _{0.72}] (Si ₈ O ₂₀)(OH) ₄	(NaF) _{0.94} (MgF ₂) _{2.3} (MgO) _{2.7} (SiO ₂) ₈
O	21.10 (± 15% error)	22.80 (± 9% error)
Na	0.72 (± 13% error)	0.94 (± 19% error)
Mg	0.35 (± 21% error)	5.00 (± 10% error)
Al	2.90 (± 13% error)	--
Si	8.00 (± 13% error)	8.00 (± 22% error)
Fe	0.63 (± 52% error)	--
F	--	5.50 (± 31% error)

There are three principal sources for variability of composition in natural C-Na⁺ and semi-synthetic ME-100 clays: (a) non-uniform atomic substitution in the crystalline cells, (b) a tendency of natural clays to vary composition within each particle, and (c) presence of impurities. Owing to the latter, in natural clays the scatter of ±15% has been reported. Variability in ME-100 is larger than the error of measurements what also reflects on the local variation of composition. The chemical heterogeneity may cause batch-to-batch variability of the mechano-chemical sensitivity during CPNC compounding, degradability, weatherability, sensitivity or lack of it toward antioxidants and stabilizers, etc.

Purification of natural clays into polymer-grade materials is a complex process with about 300 steps. The patents specify that the product should contain ≥ 5 wt% of impurities, > 300 nm large^[5]. The following minerals were identified in C-Na⁺: vermiculite, quartz, cristobalite, rutile, albite, microcline, aragonite, vaterite, dolomite, gypsum, anhydrite, alunite and sylvite. As expected, the semi-synthetic ME-100 contained traces of contaminants brought in with talc: vermiculite and gypsum. It is noteworthy that the presence of particulates, incompatible with the matrix polymer, reduces the film mechanical performance as well as its barrier properties.

CPNC

Clay dispersion in SSE or TSE resembles that of

two-phase polymer blend, thus thermodynamic interactions and complex flow field (shear, chaotic and extensional mixing) are of key importance^[6,7]. In CPNC, the interactions between phases are modified by the presence of intercalant and compatibilizer, as well as by the clay high surface energy, which leads to adsorption-&-solidification of organic molecules. Such adsorption has been observed directly using the surface force analyzer (SFA) and the small angle neutron scattering (SANS) methods^[8-11]. Also molecular dynamics computations predict formation of a solidified layers^[12-14], i.e., in the *z*-direction perpendicular to clay surface there are two layers with reduced molecular dynamics: *z*₁ ≈ 2-9 nm thick solid layer followed by *z*₂ - *z*₁ = 100-120 nm thick layer where molecular mobility progressively increases from *z*₁ to *z*₂. Luengo *et al.* determined that on a freshly cleaved mica flake polybutadiene (PBD) form layers 5-6 and 100 nm thick, respectively. Thus, the bulk behavior of PBD was observed at *z*₂ ≥ 106 nm.

The CPNC tensile and flexural properties (*i.e.*, modulus and strength) are proportional to each other^[15]. At low clay loadings the relative modulus follows the linear dependence:

$$E_R \equiv E_c / E_m = 1 + a_w w(\text{wt}\%) \quad (1)$$

(subscripts *c* and *m* stand for composite and matrix, respectively). For CPNC with PA or PP matrix *a*_w ≈ 0.2, thus at 5 wt% clay the modulus doubles. In elastomers the clay effect is larger: *a*_w ≈ 0.7. Factorial analysis at constant clay loading shows that *E*_R linearly increases interlayer spacing, *d*₀₀₁.

The tensile strength theory predicts that relative strength:

$$\theta_R \equiv \theta_c / \theta_m \leq 1 + \phi_f (\theta_f / \theta_m - 1) \quad (2)$$

where ϕ_f is clay volume fraction. Because of polymer solidification on clay, the experimental σ_R values for CPNC with PA-6 or PP are 9 and 5 times larger than predicted by eq. 2. At low clay content, the rigidity and strength linearly increases with the degree of exfoliation.

HIGH PRESSURE DILATOMETRY (HPD)

Transitions

Within the range from 0 (K) to polymers decomposition temperature there are several transitions. Of these, the melting, *T*_m, and the glass transition, *T*_g, tem-

peratures are best known. In addition there are smaller ones detectable on the derivative properties, such as compressibility or the thermal expansion coefficients (κ and α , respectively):

$$\kappa \equiv (\partial \ln V / \partial P)_{T, P^0, q}; \quad \alpha \equiv (\partial \ln V / \partial T)_{T^0, P, q} \quad (3)$$

where P^0 and T^0 are solidification pressure and temperature, respectively, and q is the rate of heating or compressing.

The lowest, quantum transition at $T < 80$ K, was predicted by Simha *et al.*^[16]. Above it, but still below T_g there are other glass-glass transitions, identified by the letters of Greek alphabet^[17]. Of these $T_\beta \approx 0.8 T_g$ is the most important as it limits the region of physical aging of vitreous materials^[18]. Next, above T_g there is the liquid/liquid or cross-over transition, $T_c/T_g \approx 1.15 - 1.35$. The magnitude of this ratio seems to depend on the fragility index, thus on rigidity of the macromolecular chain and its molecular weight^[19]:

$$m = \left(\frac{1}{T_g} \right) \left(\frac{d \log \eta}{d(1/T)} \right)_{T=T_g} \quad (4)$$

The T_c transition is readily observed by SANS and

other vibrational spectra, as well as in dielectric or rheological measurements, but not directly in *PVT*. The mode-coupling theory (MCT) considers liquid as an assembly of particles enclosed in cages formed by their neighbors with α -relaxation controlling the behavior. Only at $T > T_c$ the molecular vibrations dominate. Götze and Sjogren wrote: " T_c seems to be an equilibrium parameter of the system, which separates the supercooled liquid state in two regions"^[20]. Above T_g the semi-crystalline polymers have a dual nature, being in part molten and in part crystalline; in most $T_m \approx 1.5 T_g$ ^[21].

Determination of *PVT*

The HPD is used for determining the *PVT* surface in $V = V(T, P)$ coordinates with accuracy of 0.0002 ml/g. The specimens are tested within the range of temperatures, $T = 300-590$ K, and pressures, $P = 0.1$ to 190 MPa. The measurements are automatic, either increasing or decreasing T and P in steps. Depending on the selected rate the measurement of 350 to 750 data points the test lasts 16 to 36 h. The four procedures used for *PVT* tests are listed in TABLE 4.

The "standard" and the isobaric cooling tests show

TABLE 4 : Procedures of *PVT* measurements

Procedures	Constant variable	Adjusted variable
#1 Isothermal heating ("standard")	T is kept constant until P -sweep is completed, then increased to another level between the ambient and the maximum level, T_{max} .	P increases from 10 to 200 MPa.
#2 Isothermal cooling	Initially $T \approx T_g + 30$ °C is constant until P -sweep is completed, then decreased to another level toward the ambient T	P increases from 10 to 200 MPa.
#3 Isobaric heating	P is kept constant until T -sweep is completed, then increased to another level between 10 and 200 MPa	T increases from ambient to T_{max} .
#4 Isobaric cooling	P is kept constant until T -sweep is completed, then increased to another level between 10 and 200 MPa	T decreases from $T \approx T_g + 30$ °C to ambient

Note: As P increases the adiabatic heating increases the set T by up to 5°C. The experiments may also be conducted reducing P .

large transitory regions below T_g . Only the isobaric heating (Figures 2 and 3) shows a regular behavior with nearly constant slopes (a measure of the thermal expansion coefficient, α) in the vitreous and molten phase. Different procedures are used for different purposes. Thus, the "standard" procedure is used for easily degradable polymers, as here the specimens see the highest temperature only at the end. The isobaric cooling from $T \approx T_g + 30$ °C has been used for studying the thermodynamics of glass transition^[22].

Effects of clay, intercalants and compatibilizers

Since the expandable clay is hygroscopic (ca. 7

wt% moisture), CPNC samples must be vacuum dried^[23]. Commercial organoclay contain up to 40 wt% excess of intercalant with relatively high free volume content that affects *PVT* behavior. Highly polar PA-6 strongly interacts with crystalline clays having high surface energy^[24]. The interactions are so strong that PA-6 expels intercalant from clay surface forming 4–6 nm thick solid layer of polymer, followed by about 100 nm thick layer of organic molecules with increasing mobility as the distance from clay surface increases^[25]. The adsorption and solidification reduce the free volume by ca. 15%. In CPNC, polymer and organoclay are thermodynamically immiscible and must be compatibilized.

Microreview

The statistical thermodynamic considers clay platelets and polymer segments as statistical elements of the network, thus for exfoliation miscibility is required. Since macromolecular diffusion into clay galleries reduces the system entropy, $\Delta S < 0$, the miscibility might be expected only if the enthalpy is negative, $\Delta H < 0$, *i.e.*, if the specific (thermodynamic) interactions are strong^[26].

Derivatives, compressibility and thermal expansion coefficient

The raw data that come from HPD usually have well defined, constant P -values, but due to the adiabatic heating, T is different at each P level. Thus, if the derivatives α and κ are required, one needs to have evenly spaced data points at constant T and P . Three methods have been used to accomplish this, *viz.*, fitting the data to a polynomial, to the Tait equation^[27,28], or data interpolation to the same T -value at $P = \text{constant}$. When the derivatives are used for detecting small transitions, only the latter method is acceptable^[29].

A numerical differentiation of dependencies displayed in Figure 2 leads to the temperature-dependent thermal expansion and compressibility coefficients presented in Figures 3 and 4, respectively. The simplest α -dependencies were obtained by isobaric heating at a rate of 2°C/h. Figures 3 and 4 show that while the thermal expansion coefficient, $\alpha = \alpha(T)$ is nearly T -independent within the vitreous and molten phase, the compressibility coefficient, $\kappa = \kappa(T)$ increases in both phases. Owing to slow T change during these tests, in Figures 2 – 4 there is a weak evidence for the presence of T_c transition at 475 ± 5 K. As the new research

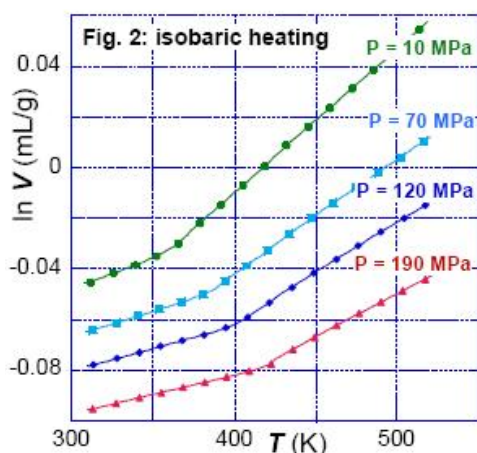


Figure 2 : PVT dependence of polystyrene (PS) measured by isobaric heating. One-in-five points are shown.

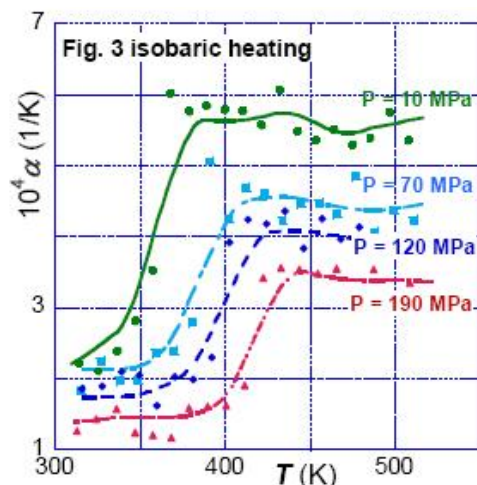


Figure 3 : Volumetric thermal expansion coefficient vs. T , computed from data in Figure 2.

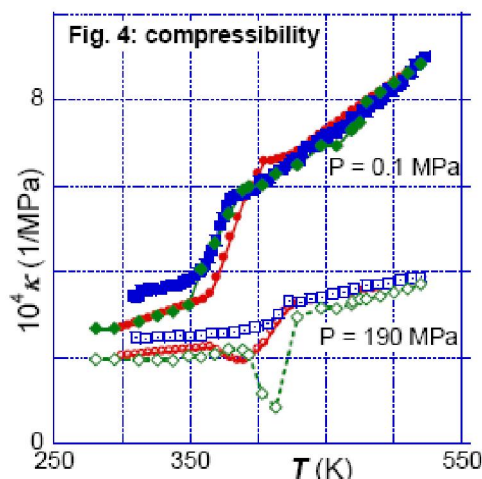


Figure 4 : Compressibility vs. T determined by the standard method (circles), isobaric heating & cooling (squares & diamonds).

shows, in the vicinity of T_g the heating or cooling rate is responsible for the polymer behavior on both sides of that transition; the effect related to the non-equilibrium fractal structures below T_c ^[30,31].

CPNC was melt compounded from PS-with 0 – 17.1 wt% of Cloisite[®]10A organoclay in a TSE^[32-34]. The HPD data were obtained using the “standard” PVT procedure; Figures 5 and 6 display α as function of P , T and w . In the vitreous state α_g shows two types of behavior. For clay loadings $w \leq 2$ wt% it has low value, decreasing with P to about zero, whereas for $w > 3.6$ wt% its values are negative, *i.e.*, heated specimen shrinks with increasing T , instead of expanding. The magnitude of α_g at $T < T_g$ strongly depends on the cooling process from the melt. In the molten state the isobaric val-

ues of α_m are nearly constant, independent of T . Addition of clay reduces α_g in the full range of P . In the vicinity

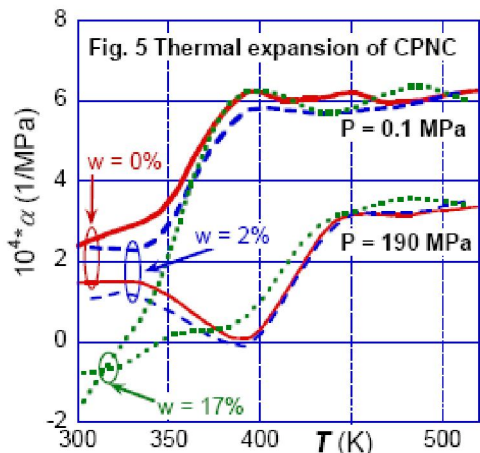


Figure 5: Temperature dependence of the volumetric thermal expansion coefficient at two pressures and four concentrations.

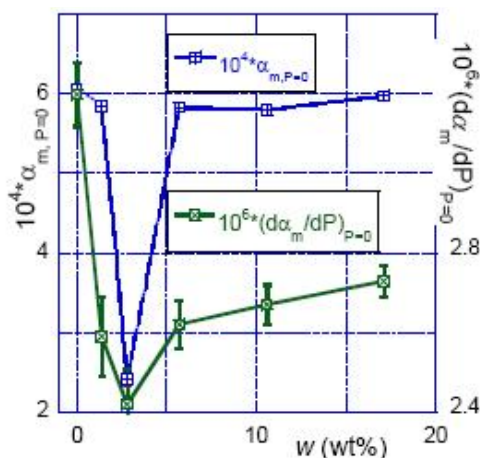


Figure 6: The thermal expansion coefficient at $T > T_g$ and its pressure gradient as function of clay concentration, w .

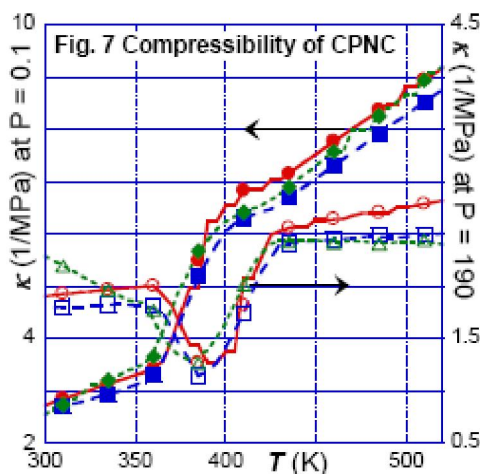


Figure 7: Compressibility coefficient vs. T at $P = 0.1$ and 190 MPa for PNC containing: $w = 0, 2$ and 17 wt%.

of $w_2 = 3.6$ wt% the function takes a dip. A similar, but stronger local decrease is observed in the melt; Figure 6 displays $\alpha_m = \alpha_m(w)$ at ambient pressure and its pressure gradient. Figure 7 shows κ as functions of P , T and w . By contrast with α , the compressibility tends to increase with T , while its temperature dependence decreases with P virtually to zero at the highest P and w . The $\kappa = \kappa(w)$ dependence also goes through a local minimum near $w_2 = 3.6$ wt%.

Effect of clay on α and κ in PA-6 based PNC

Dry PA-6 has $T_g(\text{PA-6}) \approx 323$ and $T_m(\text{PA-6}) \approx 500$ K, both dependent on P as well as on the method of material preparation. The HPD measurements of PA-6, its PNC-2 and PNC-5 containing 2.29 ± 0.13 and 4.91 ± 0.24 wt% of clay, respectively (inorganic content), were carried out at $T = 300 - 580$ K and $P = 0.1 - 190$ MPa^[35]. The derivatives α and κ were computed by numerical differentiation of the PVT isobaric

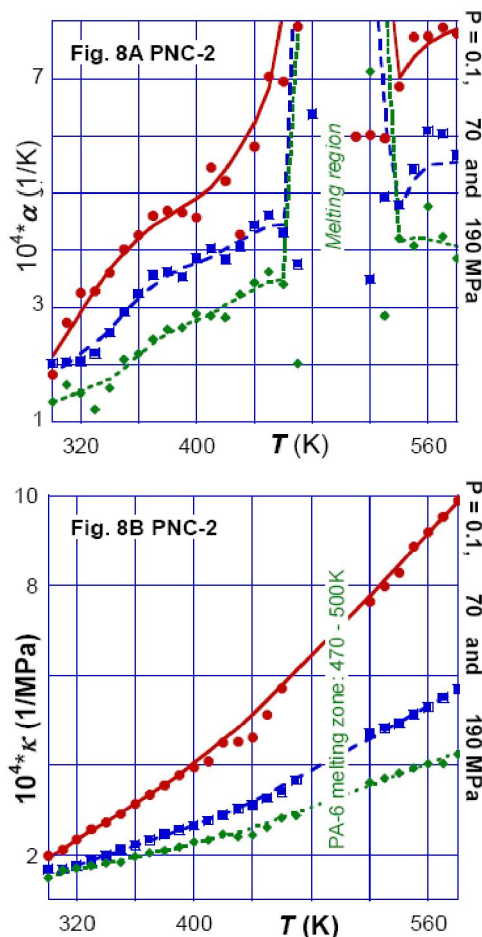


Figure 8: The thermal expansion and compressibility coefficients vs. T at $P = 0.1 - 190$ MPa for PA-6 nanocomposite with 2 wt% clay, PNC-2.

Microreview

or isothermal data. As shown in Figure 8, the attention focused on T_m region and its variation with P , T and w . The thermal expansion coefficient for the crystalline phase of PA-6 and its PNCs is separated from the melt by a “chimney-like” melting zone. The addition of clay reduces α of the solid phase, and increases its value in the melt. This behavior might be related to the presence of high crystallinity regions in the vicinity of the MMT high energy surface. By contrast with α the $\kappa = \kappa(T)$ function for PA-6 and its PNCs follows the same dependence on both sides of T_m (theoretically predicted)^[36,37]. The low- P compressibility slightly increases with organoclay content, what may be related to the intercalant presence.

THERMODYNAMIC THEORIES

The presented α and κ values were numerically calculated from the HPD data, on purpose not involving any theoretical model or assumption. However, since an adequate theory may lead to determination of the interaction parameters, cohesive energy density, internal pressure, and the free volume content, a short discussion is instructive. Furthermore, the theoretical analysis of CPNC behavior offers an insight into the non-equilibrium phenomena, such as diffusivity, rheology, positron annihilation lifetime spectroscopy (PALS), etc.^[38].

Simha-Somcynsky cell-hole theory

The Simha and Somcynsky (S-S) cell-hole theory is based on the lattice-hole model^[39,40]. The molecular segments of s -mer occupy y -fraction of the lattice sites, while the remaining randomly distributed sites, $h = 1 - y$, are left empty accounting for the free volume. The theory was derived assuming thermodynamic equilibrium. Furthermore, postulating that at $T < T_g$ a part of the free volume is frozen, the theory was later extended to the vitreous and semi-crystalline non-equilibrium states^[41].

The derivation starts with the configurational partition function, which incorporates the Lennard-Jones (L-J) potential with two interaction parameters: the maximum attractive energy, ε^* , and the segmental repulsion volume, v^* . Next, assuming validity of the corresponding states principle (CSP), the variables are divided by

the characteristic reducing parameters:

$$\left. \begin{aligned} \tilde{V} &\equiv V/V^* \\ \tilde{T} &\equiv T/T^* \\ \tilde{P} &\equiv P/P^* \end{aligned} \right\} \Rightarrow M_s \frac{P^* V^*}{RT^*} = \frac{c}{s} \Leftarrow \begin{cases} P^* = zq\varepsilon^*/(sv^*) \\ T^* = zq\varepsilon^*/(Rc) \\ V^* = v^*/M_s \end{cases} \quad (5)$$

where $zq = s(z - 2) + 2$ is the number of interchain contacts between s segments (each of molecular weight: $M_s = M_n/s$) in a lattice of the coordination number z , and $3c$ is the number of the external degrees of freedom. The reduced free volume function is a volume-average of the solid-like and gas-like contributions. From the configurational Helmholtz free energy S-S derived the equation of state (eos), the cohesive energy density, CED, solubility parameter, $\delta = \delta(T, P)$, and the internal pressure, \tilde{p}_i ^[42-45].

Next, the S-S theory for a single component liquid was applied to the homogeneous, binary mixtures, postulating that there is only one type of vacancies and one cell size for the components^[46,47]. The average interaction parameters $\langle \varepsilon^* \rangle$ and $\langle v^* \rangle$ are related to binary ones via:

$$\langle \varepsilon^* \rangle \langle v^* \rangle = \sum_{i,k} X_i X_k \varepsilon_{i,k}^* (v_{i,k}^*)^m; \quad m \in (2, 4) \quad (6)$$

where the two values of m reflect the assumed Lennard-Jones 6-12 potential. The S-S theory for multicomponent systems well describes the phase equilibria, CED, solubility as well as PVT behavior of polymer mixtures with gases, liquids^[48], solids^[49-51] and nanocomposites^[52,53].

Figures 9A and 9B respectively illustrate the effect of clay content on the free volume parameter h and the L-J interaction parameters in molten PNC with PS matrix. At constant clay loading of 2 wt% adsorption-&-solidification of polymer linearly reduces the free volume content with the interlayer spacing, d_{001} ^[32]:

$$\Delta h = 2.51 + 0.833d_{001}; \quad r = 1.000 \quad (7)$$

Because of the favorable thermodynamic interactions between clay and PA-6 these CPNCs are exfoliated, at 2 wt% clay h is reduced by 15%. The functions: h , $\langle \varepsilon^* \rangle$ and $\langle v^* \rangle$ vs. w go through a local extrema at $w_2 = 3.6$ wt% clay – further addition of organoclay reduces the interlayer spacing and dilutes the intercalated stacks. The effect parallels the behavior of derivative properties on clay content shown in Figures 6 and 7.

The old notion of the structure presence in molten polymers is now accepted on the theoretical and experimental basis. The twinkling fractal theory (TFT) of the glass transition and recent atomic force microscopy (AFM) in the tapping-mode^[54,55] are convincing proofs of the dynamic, solid aggregate presence below and above T_g – only above the crossover temperature, T_c , the true liquid-like behavior was found. The detailed analysis of data from HPD, as well as dynamic shear tests of PS indicate the presence of a transient structure on both sides of T_g ; hence, molten polymer not always is at thermodynamic equilibrium. For example, the difference of rigidity in quenched and annealed specimens was detectable at $T = T_g + 20^\circ\text{C}$, i.e., half way to $T_c = 419 \pm 2 \text{ K}$, or $T_c/T_g = 1.16 \pm 0.01$. However, with time the structure tends toward an “equilibrium” value specific for given set of conditions – an effect semblable to physical aging below T_g ^[18].

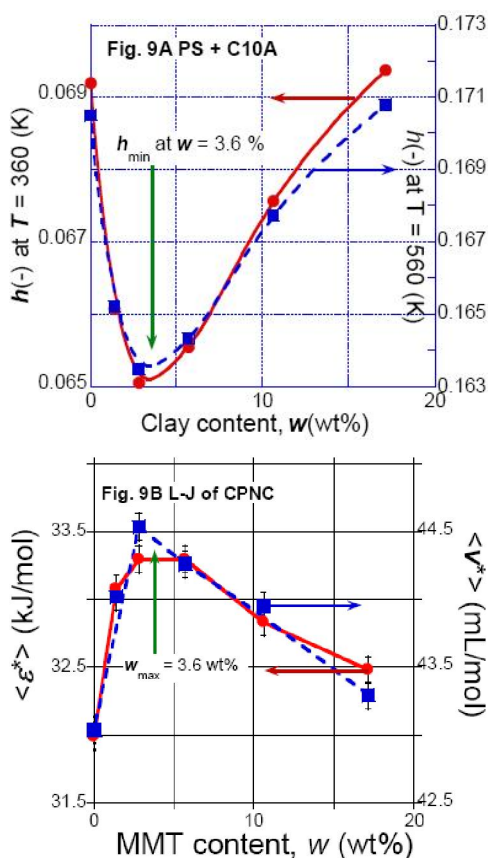


Figure 9 : Free volume and the L-J interaction parameters (Figure 9B) vs. clay content for PS-based CPNC at $P = 0.1 \text{ MPa}$ and $T = 360$ and 560 (K) .

Analysis of the PVT surface by means of the S-S eos leads to the hole content, h , which should correlate

with liquids viscosity following the dependence^[56-59]:

$$\ln \eta_{\sigma_{ij}=\text{const}} = a_0 + a_1 Y_s; Y_s \equiv 1/(h + a_2) \quad (8)$$

The relation was found valid for low molecular weight n -paraffins or silicon oils within the ranges of $T = 20$ to 204°C and $P = 0.1$ to 500 MPa , with constants: $a_1 = 0.79 \pm 0.01$ and $a_2 = 0.07$. However, it failed when applied to data of eight molten polymers, whose PVT and $\eta = \eta(P, T)$ were measured^[60]. The discrepancy is related to the presence of structures in the latter systems at $T_g \leq T \leq T_c \approx T_{LL}$, postulated by Boyer and his colleagues 40 years ago; only above T_{LL} the processing would yields articles with smooth surface and good, reproducible performance^[61,62].

The vitreous region

Properties of the vitreous phase depend on the way it was achieved^[63]. The analysis followed the procedure developed by Simha and his colleagues^[64-66]. Accordingly, the free volume frozen fraction, FF , was computed from the relation:

$$FF = 1 - (\partial h / \partial T')_{P, \text{glass}} / (\partial h / \partial T')_{P, \text{extrapol}} \quad (9)$$

Figure 10 displays the $FF = FF(w)$ dependence of CPNC = PS + C10A at several pressures. Only at $w < w_2 = 3.6 \text{ wt}\%$, $FF < 1$ is found, while at higher clay concentration $FF > 1$. This behavior stems from the adsorption-&-solidification of PS on clay during melt quenching from $T > T_g + 50^\circ\text{C}$.

MNSJ equation of state for semi-crystalline CPNC

The thermodynamic theory for semi-crystalline polymers borrows from several sources: the quantum theory of polymeric glasses at $T = 80 \text{ K}$ ^[16], the cell model for crystalline polymers^[67], and several later refinements^[68,69]. The cell lattice assumes absence of holes, thus the reducing parameters (P^* , T^* , V^*) are different than those computed using S-S eos cell-hole theory for equilibrium liquids. The theory is valid for the crystalline phase at $T_g \leq T (\text{K}) \leq T_m$. The applicability for describing the PVT dependencies has been examined first for neat PE and PA-6 and then for CPNC. In the PA-6 systems the additivity of crystalline and non-crystalline domains was assumed. The sequence of the computation steps and the assumed models are detailed in the original publications^[35-37]. Figure 11 displays the final fit of the

Microreview

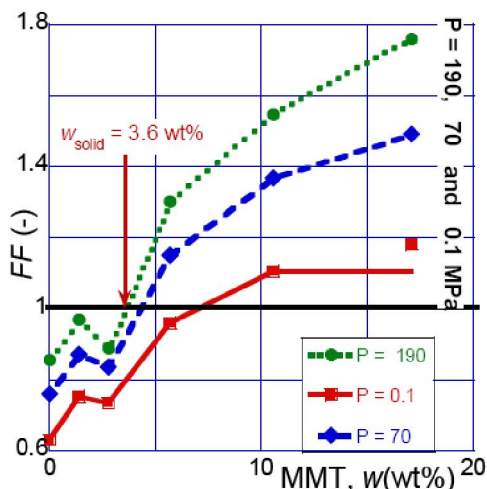


Figure 10 : Free volume frozen fraction, $FF = FF(w)$, for PS-1301 with 0 – 17 wt% of C10A at the selected (for clarity) three pressures, $P = 0.1 - 190$ MPa. See text.

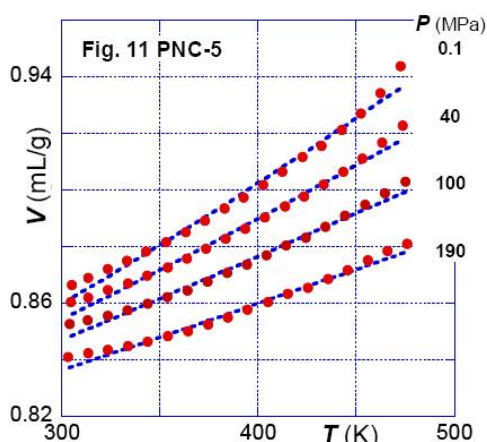


Figure 11 : Specific volume of PA-6 with 5 wt% clay at $P = 0.1 - 190$ MPa. Points are experimental and lines computed from the Midha–Nanda–Simha–Jain (MNSJ) theory.

theory to HPD data.

Interaction coefficients

The L-J potential with adjustable exponents: $m = 10 - 13$, $n = 6 - 7$ was cast into the present form of the “6-12 potential” after the quantum mechanics showed that the attractive forces between hydrogen atoms follow the separating distance with $n = 6$, and the repulsive interactions with $m = 2n$ ^[70]. The 6-12 potential was incorporated into the S-S and MNSJ theories. For a single component, the intersegmental L-J interaction parameters are ϵ^* and v^* , whereas those for multi-component systems are averages, $\langle \epsilon^* \rangle$ and $\langle v^* \rangle$. For extracting the individual binary interactions from these latter ones Eq. 6 should be solved.

The situation is relatively simple for immiscible binary polymer blends, where properties of each component directly can be measured, and only the heterogeneous ones, ϵ_{ij}^* and v_{ij}^* (i.e., polymer-*i* with polymer-*j*), must be determined from the blend behavior. However, it is noteworthy that such a treatment ignores the presence of the interphase whose importance increases with the enhanced dispersion^[71].

CPNCs are more complex systems than blends as they comprise matrix, nano-sized particles, intercalant, compatibilizer(s) and various industrial additives. Furthermore, the clay usually exists in a wide spectrum of dispersions ranging from full exfoliation to micron-size aggregates. Clay also adsorbs the organic phase creating a gradient of molecular mobility stretching up to 120 nm from the clay surface. During the last 20 years CPNCs with immiscible polymer blends became of interest^[72]. Thus, it is a challenge to convert these systems into a model binary mixture of matrix and solid particles that realistically will represent the physical behavior. In other words, the CPNC model should specify the composition of the matrix and dispersed solid phase. For computation,

- The solid particles are assumed comprising clay platelets with $z_1 \approx 4-6$ nm thick, solidified organic layer with the interaction parameters ϵ_{22}^* and v_{22}^* .
- The matrix consists of the organic layer at $z > z_1$, with ϵ_{11}^* and v_{11}^* .

In consequence, the model implicitly assumes that the L-J parameters depend on the clay content, limited to the low clay content, $w < w_2 = 3.6$ wt%^[53].

Because of differences in clay-polymer interactions, one should not presume that a single model will be applicable to all CPNC. For example, owing to polarity of PA-6 and strong interaction with the negatively charged clay platelets, the PA-6 based CPNC are relatively easily exfoliated by the synthetic or compounding method. However, since the intercalant location and molecular structure are different than that observed in PS or polyolefin (PO) matrix, the model for extracting the L-J parameter should account for the difference^[15]. Flow analysis of the PA-6 based CPNC led to the “hairy clay particles” (HCP) model^[73]. By contrast, the nanocomposites with polyolefin or PS matrix, which does not bond to clay surface, are immiscible with most

intercalants and need a compatibilizer or two. Therefore, before devising a realistic model for the tested PNC, information about composition, thermodynamic interactions and degree of dispersion is needed^[52].

For CPNCs out of the six parameters of Eq. 6 only two (ϵ_{11}^* and v_{11}^*) may be measured directly. The two cross-interaction parameters, ϵ_{12}^* and v_{12}^* , are calculated following the Berthelot's rule and the algebraic average, respectively:

$$\epsilon_{12}^* = (\epsilon_{11}^* \epsilon_{22}^*)^{1/2} \quad \text{and} \quad v_{12}^* = [v_{11}^{*1/3} + v_{22}^{*1/3}]^3 / 8 \quad (10)$$

The remaining two parameters, ϵ_{22}^* and v_{22}^* , are then calculable from the average interaction expressions.

Figure 12 displays the concentration dependence of ϵ_{22}^* for PS-based CPNC. The broken line represents the dependence with the expected maximum at the critical concentration, $w_2 = 3.6$ wt%^[52]. Figure 13 shows the binary interaction parameters in the full range of the (linear not volumetric) clay concentration ($w = 0 - 100$ wt%) for PP-based CPNC with C20A. The computations lead to ϵ_{11}^* and v_{11}^* for all points, excepting the two last ones at $w = 100$ wt% clay corresponding to ϵ_{22}^* and v_{22}^* . From these two sets of numbers the cross-interactions, ϵ_{12}^* and v_{12}^* , may be calculated. The theory also suggests that the L-J parameters may not be independent, viz. $\epsilon^* \propto v^* P^*$ ^[45]. The empirical relation for PS and its CPNC is: $\epsilon^* \cong 13.4 + 0.445v^*$; $r = 0.95$.

The binary interaction parameters for the matrix (ϵ_{11}^* , v_{11}^*) and for the solid phase (ϵ_{22}^* , v_{22}^*) are listed in TABLE 5. It may seem odd that the difference between the interaction parameters of the matrix and solid part is so

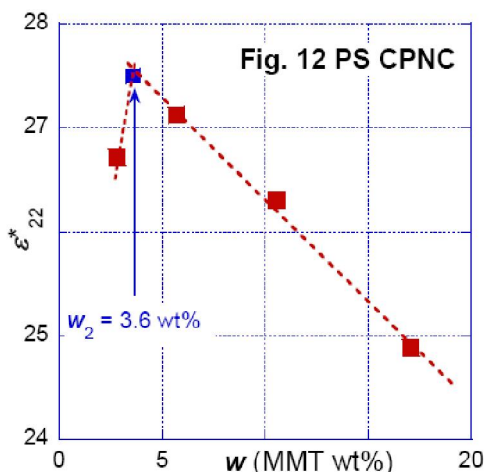


Figure 12 : Computed stack-stack interaction for intercalated PS-based CPNC.

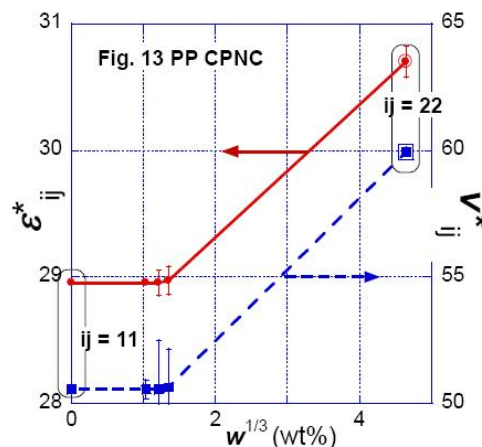


Figure 13 : L-J interaction parameters for PP-based CPNC.

TABLE 5 : The binary interaction parameters for PNC with PA-6, PP and PS matrix.

Polymer	Matrix		Solid		Refs.
	ϵ_{11}^*	v_{11}^*	ϵ_{22}^*	v_{22}^*	
PA-6	34.1 ± 0.3	32.0 ± 0.1	31.2 ± 0.3	25.9 ± 0.3	[35]
PP	28.9 ± 0.1	50.6 ± 0.4	30.7 ± 0.4	59.9 ± 0.3	[53]
PS	32.0 ± 0.6	43.0 ± 1.7	33.0 ± 0.1	44.2 ± 0.1	[52]

small. However, the definition of solids is a clay platelet enrobed with an organic phase, thus there are no clay-clay interactions, but rather those between polymeric solid layers adsorbed on the clay platelets and the polymeric matrix.

THEORETICAL PREDICTIONS

Theories are built assuming that a model system on the one hand simulates the phenomenon and on the other it permits comparison with experimental results. The notorious assumption of most polymer theories is an omission of polydispersity, the presence of additives and the non-random distribution of properties, e.g., introduced by mixing, forming or temperature gradients. Furthermore, the thermodynamics theories usually assume equilibrium.

The S-S and MNSJ equations of state predict the PVT variability of, respectively, amorphous and semi-crystalline molten polymer and their α and κ derivatives. The theories are cast in reduced form, thus they are universally applicable to any system with known set of the reducing parameters, P^* , T^* and V^* (viz. Eq. 5). Figures 14A and 14B show, respectively, the α and κ dependencies for PA-6 at, e.g., $T = 5 - 284^\circ\text{C}$, $P =$

Microreview

25 – 314 MPa, $10^4\alpha = 3.35 - 8.02$ (1/K) and $\kappa = 0.13 - 1.01$ (1/kPa). Thus, indeed these values are well within the experimental magnitudes measured for these coefficients. Similarly good representation of the experimental data was obtained for PS at $T = 20 - 313^\circ\text{C}$, $P = 11 - 189$ MPa, where $10^4\alpha = 3.52 - 8.44$ (1/K) and $\kappa = 0.07 - 0.60$ (1/kPa).

The S-S eos well describes the PVT behavior of amorphous polymers up to the second volume derivatives. The experimental PA-6 data were compared with a theoretical model assuming dispersion of PA-6 crystals in its melt. Accordingly, the applied MNSJ and S-S

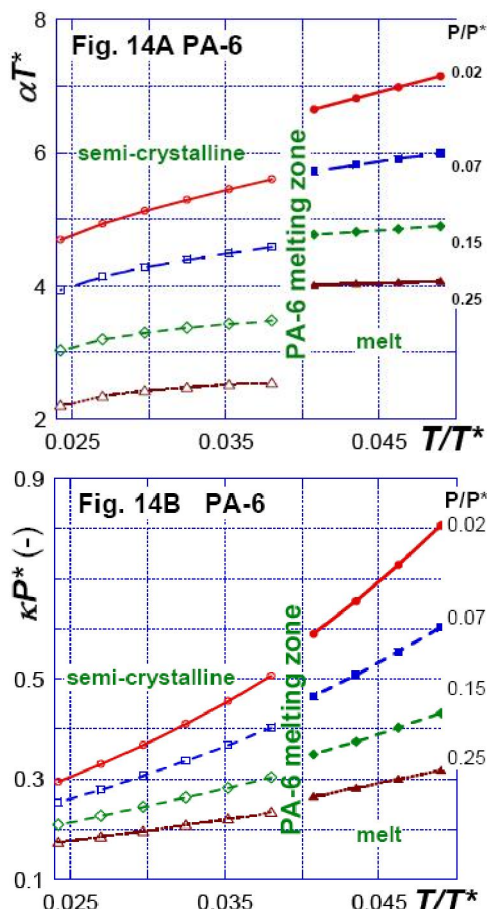


Figure 14 : Theoretical predictions of the thermal expansion and compressibility coefficients in reduced variables for a semi-crystalline/molten polymeric system computed from a combination of S-S and MNSJ eos^[36,37].

theories, respectively, showed excellent agreement with the experimental data.

SUMMARY AND CONCLUSIONS

This review discussed three aspects of CPNC:

- **Characterization of clays:** Properties of the natural clays significantly vary with the geographical location and mine strata. The differences are in: platelet shape, size and size distribution, chemical composition and the presence of contaminants.
- **HPD measurements, thermodynamic theories and binary interactions:** Of the four HPD test procedures the isobaric heating method is most useful, while the “standard” is recommended for the thermally unstable systems. The α and κ coefficients should be directly computed by numerical differentiation of the PVT data. As the comparison of the theoretical predictions with the experimental data of $\alpha = \alpha(T, P)$ and $\kappa = \kappa(T, P)$ shows, the amorphous and semi-crystalline PVT data well follow the S-S and MNSJ theories, respectively. For CPNC, the analysis of the HPD data by means of these theories leads to the determination of the binary matrix-clay L-J interaction parameters.
- **The non-equilibrium structures on both sides of T_g :** The demonstrated non-equilibrium nature of polymeric systems on both sides of T_g demands caution while generalizing the result. For example, a significant difference in melt behavior was observed by varying the time scale of the experiment.

REFERENCES

- [1] L.A.Utracki; Clay-Containing Polymeric Nanocomposites, RAPRA, Shawbury, UK, ISBN: 978-1-85957-488-1, (2004).
- [2] L.A.Utracki, M.Sepehr, J.Li; Intern.Polym.Process, **21(1)**, 1-14 (2006).
- [3] L.A.Utracki, M.Sepehr, E.Boccaleri; Polym.Adv. Technol., **18(1)**, 1-37 (2007).
- [4] L.A.Utracki, W.Broughton, N.Gonzalez Rojano, L.Carvalho, C.A.Achete; Polym.Eng.Sci., **51(4)**, 559-572 (2011).
- [5] M.Clarey, J.Edwards, S.J.Tsipursky, G.W.Beall, D.D.Eisenhour; Method of Manufacturing Polymer - Grade Clay for Use in Nanocomposites, US Pat., 6,050,509, (2000).
- [6] L.A.Utracki, (Ed); Polymer Blends Handbook, Kluwer, Dordrecht, ISBN: 978-0-306-48244-1, (2002).
- [7] W.Song; SPE ANTEC, Techn.Pap., **46(1)**, 270-275 (2000).

- [8] J.N.Israelachvili, M.Tirrell, J.Klein, Y.Almog; *Macromolecules*, **17**(2), 204-209 (1984).
- [9] R.G.Horn, J.N.Israelachvili; *Macromolecules*, **21**(9), 2836-2841 (1988).
- [10] T.Cosgrove, T.G.Heath, K.Ryan, T.L.Crowley; *Macromolecules*, **20**(11), 2879-2882 (1987).
- [11] T.Cosgrove, T.G.Heath, T.J.S.Phipps, R.M.Richardson; *Macromolecules*, **24**(1), 94-98 (1991).
- [12] G.Fleer, M.A.Cohen-Stuart, J.M.H.M.Scheutjens, T.Cosgrove, B.Vincent; *Polymers at Interfaces*, Chapman and Hall, London, (1993).
- [13] R.Hentschke; *Macromol.Theory Simul.*, **6**(2), 287-316 (1997).
- [14] Y.Termonia; *Polymer*, **50**(4), 1062-1066 (2009).
- [15] M.Tokihisa, K.Yakemoto, T.Sakai, L.A.Utracki, M.Sepchr, J.Li, Y.Simard; *Polym.Eng.Sci.*, **46**(8), 1040-1050 (2006).
- [16] R.Simha, J.M.Roe, V.S.Nanda; *J.Appl.Phys.*, **43**, 4312-4317 (1972).
- [17] (a) R.F.Boyer; *J.Macromol.Sci.-Phys.*, **B183**, 461-553 (1980); (b) R.F.Boyer; Evidence from T_{LL} and Related Phenomena for Local Structure in the Amorphous State of Polymers, in *Order in the Amorphous State*, R.L.Miller, J.K.Rieke, (Eds); New York: Plenum, (1987).
- [18] L.C.E.Struik; *Physical aging in Amorphous Polymers and Other Materials*. Amsterdam: Elsevier, (1978).
- [19] N.V.Surovtsev; *J.Phys.: Condens.Mater.*, **19**, 196101, (2007).
- [20] W.Götze, L.Sjogren; *Rep.Prog.Phys.*, **55**, 241-370 (1992).
- [21] R.F.Boyer; T_{LL} and Related Liquid State Transitions-Relaxations: A Review, in *Polymer Yearbook 2*, R.A.Pethrick, (Ed); Chur-London-Paris-New York: Harwood Academic Publishers, (1985).
- [22] (a) A.Quach, R.Simha; *J.Appl.Phys.*, **42**, 4592-4606 (1971); (b) A.Quach, R.Simha; *J.Phys.Chem.*, **76**, 416-421 (1972).
- [23] L.A.Utracki, R.Simha, A.Garcia-Rejon; *Macromolecules*, **36**(6), 2114-2121 (2003).
- [24] G.Tanaka, L.A.Goettler; *Polymer*, **43**(2), 541-553 (2002).
- [25] G.Luengo, F.-J.Schmitt, R.Hill, J.N.Israelachvili; *Thin Film Rheology and Tribology of Confined Polymer Melts: Contrasts with Bulk Properties*, **30**(8), 2482-2494 (1997).
- [26] K.Kim, L.A.Utracki, M.R.Kamal; *J.Chem.Phys.*, **121**, 10766-10777 (2004).
- [27] P.G.Tait; On Some of the Physical Properties of Fresh Water and of Sea-Water, in Report on the Scientific Results of the Voyage of H.M.S. Challenger, C.W.Thomson, (Ed); *Physics and Chemistry*, **2**(4), 1 (1889).
- [28] V.S.Nanda, R.Simha; *J.Chem.Phys.*, **41**, 1884-1885 (1964).
- [29] L.A.Utracki; PVT Characterization of Polymeric Nanocomposites, Chapter 2 in *Characterization Techniques of Polymer Nanocomposites*, V.Mittal, (Ed); Wiley VCH Verlag, Weinheim, Germany, (2012).
- [30] R.P.Wool; *J.Polym.Sci.Part B Polym.Phys.*, **46**, 2765-2778 (2008).
- [31] L.A.Utracki, P.Sammut; *J.Polym.Sci.Part B: Polym.Phys.*, **49**, 1369-1380 (2011).
- [32] S.Tanoue, L.A.Utracki, A.Garcia-Rejon, J.Tatibouët, K.C.Cole, M.R.Kamal; *Polym.Eng.Sci.*, **44**(6), 1046-1060 (2004).
- [33] S.Tanoue, L.A.Utracki, A.Garcia-Rejon, P.Sammut, M.-T.Ton-That, I.Pesneau, M.R.Kamal, J.Lyngaae-Jørgensen; *Polym.Eng.Sci.*, **44**(6), 1061-1076 (2004).
- [34] S.Tanoue, L.A.Utracki, A.Garcia-Rejon, J.Tatibouët, M.R.Kamal; *Polym.Eng.Sci.*, **45**(6), 827-837 (2005).
- [35] (a) L.A.Utracki; *J.Polym.Sci.Part B: Polym.Phys.*, **47**(3), 299-313 (2009); (b) *J.Polym.Sci.Part B: Polym.Phys.*, **47**(10), 966-980 (2009).
- [36] L.A.Utracki; *European Polym.J.*, **45**(7), 1891-1903 (2009).
- [37] L.A.Utracki; *Polym.Degradation Stability*, **95**(3), 411-421 (2010).
- [38] L.A.Utracki, A.M.Jamieson, (Eds); *Polymer Physics: From Suspensions to Nanocomposites to Beyond*, New York: J. Wiley & Sons, (2010).
- [39] R.Simha, T.Somcynsky; *Macromolecules*, **2**(4), 342-350 (1969).
- [40] T.Somcynsky, R.Simha; *J.Appl.Phys.*, **42**, 4545-4548 (1971).
- [41] R.K.Jain, R.Simha; *J.Polym.Sci.: Polym.Lett.Ed.*, **17**(1), 33-37 (1979).
- [42] L.A.Utracki; *J.Polym.Sci.Part B: Polym.Phys.*, **42**(15), 2909-2915 (2004).
- [43] L.A.Utracki, R.Simha; *Polym.Int.*, **53**(3), 279-286 (2004).
- [44] L.A.Utracki, R.Simha; *J.Polym.Sci.: Part B: Polym. Phys.*, **39**(3), 342-362 (2001).
- [45] L.A.Utracki; *Polymer*, **46**(25), 11548-11556 (2005).
- [46] R.K.Jain, R.Simha; *Macromolecules*, **13**(6), 1501-1508 (1980).

Microreview

- [47] R.K.Jain, R.Simha; *Macromolecules*, **17**(12), 2663-2668 (1984).
- [48] L.A.Utracki, R.Simha; *Macromol.Theory Simul.*, **10**(1), 17-24 (2001).
- [49] R.Simha, R.K.Jain, S.C.Jain; *Polym.Compos.*, **5**(1), 3-10 (1984).
- [50] E.Papazoglou, R.Simha, F.H.J.Maurer; *Rheol.Acta*, **28**(4), 302-308 (1989).
- [51] R.Simha, E.Papazoglou, F.H.J.Maurer; *Polym.Compos.*, **10**(6), 409-413 (1989).
- [52] L.A.Utracki; *J.Polym.Sci.Part B: Polym.Phys.*, **46**(23), 2504-2518 (2008).
- [53] L.A.Utracki, R.Simha; *Macromolecules*, **37**(26), 10123-10133 (2004).
- [54] R.P.Wool, A.Campanella; *J.Polym.Sci.Part B: Polym.Phys.*, **47**(24), 2578-2590 (2009).
- [55] J.F.Stanzione III, K.E.Strawhecker, R.P.Wool; *J.Non-Crystalline Solids*, **357**(2), 311-319 (2011).
- [56] L.A.Utracki; *Polym.Eng.Sci.*, **23**(8), 446-452 (1983).
- [57] L.A.Utracki; *Canad.J.Chem.Eng.*, **61**(5), 753-758 (1983).
- [58] L.A.Utracki; *J.Rheol.*, **30**(4), 829-841 (1986).
- [59] L.A.Utracki; *Polym.Eng.Sci.*, **25**(11), 655-668 (1985).
- [60] L.A.Utracki, T.Sedlacek; *Rheologica Acta*, **46**(4), 479-494 (2007).
- [61] S.J.Stadnicki, J.K.Gillham; *J.Appl.Polym.Sci.*, **20**(5), 1245-1275 (1976).
- [62] S.E.Keinath, R.F.Boyer; *J.Appl.Polym.Sci.*, **26**(6), 2077-2085 (1981).
- [63] M.Schmidt; *Macroscopic Volume and Free Volume of Polymer Blends and Pressure-Densified Polymers*. Ph.D. Thesis, Chalmers University, Göteborg, (2000).
- [64] (a) J.E.McKinney, R.Simha; *Macromolecules*, **7**(6), 894-901 (1974); (b) *ibid.*, **9**, 430-441 (1976); (c) *J.Res.NBS – Phys.Chem.*, **81A**, 283-297 (1977).
- [65] J.G.Curro, R.R.Lagasse, R.Simha; *J.Appl.Phys.*, **52**(10), 5892-5897 (1981).
- [66] L.A.Utracki; *J.Polym.Sci.Part B: Polym.Phys.*, **45**(3), 270-285 (2007).
- [67] Y.R.Midha, V.S.Nanda; *Macromolecules*, **10**(5), 1031-1035 (1977).
- [68] R.Simha, R.K.Jain; *J.Polym.Sci.Part B: Polym.Phys. Ed.*, **16**(8), 1471-1489 (1978).
- [69] R.K.Jain, R.Simha; *J.Polym.Sci.: Polym.Phys.Ed.*, **17**(11), 1929-1946 (1979).
- [70] J.E.Lennard-Jones, A.F.Devonshire; *Proc.Roy.Soc.*, **163**(1), 53-70 (1937).
- [71] (a) L.A.Utracki; *Polymer Alloys and Blends*, Munich: Hanser Verlag, (1989); (b) L.A.Utracki, (Ed); *Polymer Blends Handbook*, Dordrecht: Kluwer Academic Pub., (2002).
- [72] L.A.Utracki; *Rheology of Polymer Blends*, in *Encyclopedia of Polymer Blends*, Chapter 2, A.Isayev, (Ed); Weinheim: Wiley-VCH Verlag, **2**, (2011).
- [73] L.A.Utracki, J.Lyngaae-Jørgensen; *Rheologica Acta*, **41**(5), 394-407 (2002).